A Small Satellite Version of a Broad-band Soft X-ray Polarimeter

Herman L. Marshall[a], Sarah N. T. Heine[a], Alan Garner[a], Eric M. Gullikson[b], H. Moritz Günther[a], Christopher Leitz[c], Rebecca Masterson[a], Eric D. Miller[a], William Zhang[d], Rozenn Boissay-Malaquin[e], Ilaria Caiazzo[f], Deepto Chakrabarty[a], Rosemary Davidson[a], Luigi C. Gallo[g], Ralf K. Heilmann[a], Jeremy Heyl[h], Erin Kara[a], Alan Marscher[j], and Norbert S. Schulz[a]

[a]MIT Kavli Institute, Cambridge, MA, USA
[b]Lawrence Berkeley National Lab, Berkeley, CA, USA
[c]MIT Lincoln Lab, Lexington, MA, USA
[d]Goddard Space Flight Center, Greenbelt, MD, USA
[e]University of Maryland Baltimore County, Baltimore, MD, USA
[f]California Inst. of Technology, Pasadena, CA, USA
[g]Saint Mary's University, Halifax, NS, Canada
[h]University of British Columbia, Vancouver, BC, Canada
[j]Boston University, Boston, MA, USA

ABSTRACT

We describe a new implementation of a broad-band soft X-ray polarimeter, substantially based on a previous design. This implementation, the Pioneer Soft X-ray Polarimeter (*PiSoX*) is a SmallSat, designed for NASA's call for Astrophysics Pioneers, small missions that could be CubeSats, balloon experiments, or SmallSats. As in *REDSoX*, the grating arrangement is designed optimally for the purpose of polarimetry with broad-band focussing optics by matching the dispersion of the spectrometer channels to laterally graded multilayers (LGMLs). The system can achieve polarization modulation factors over 90%. For *PiSoX*, the optics are lightweight Si mirrors in a one-bounce parabolic configuration. High efficiency, blazed gratings from opposite sectors are oriented to disperse to a LGML forming a channel covering the wavelength range from 35 Å to 75 Å (165 - 350 eV). Upon satellite rotation, the intensities of the dispersed spectra, after reflection and polarizing by the LGMLs, give the three Stokes parameters needed to determine a source's linear polarization fraction and orientation. The design can be extended to higher energies as LGMLs are developed further. We describe examples of the potential scientific return from instruments based on this design.

Keywords: X-ray, polarimeter, astronomy, multilayer, mirror, grating

Like true pioneers, we can explore a new frontier in astrophysics. This instrument would be the first spectropolarimeter for the soft X-ray band, the Pioneer Soft X-ray Polarimeter (*PiSoX*). Observing neutron stars with *PiSoX*, we will test the effects of vacuum birefringence, search for proton cyclotron lines, and check atmospheric models – ultimately constraining the equation of state of nuclear matter. Using *PiSoX* to observe active galaxies, we will discriminate between jet and disk models of their very soft X-ray emission, providing measures of jet magnetic fields, disk inclinations, and the importance of Comptonization. *PiSoX* will expand our view of polarized emission across the electromagnetic spectrum, complementing results from the Imaging X-ray Polarimetry Explorer (*IXPE*, 2-8 keV[1]), by measuring spectral components that cannot be examined with *IXPE*.

PiSoX is a mission made feasible by our recent technology advancements in X-ray mirrors, gratings, and multilayer mirrors. The science instrument in *PiSoX* consists of parabolic X-ray optics and Critical Angle Transmission (CAT) gratings that disperse soft X-rays to a polarizing multilayer (ML) coated mirror that then

reflects the light to a CCD detector. *PiSoX* will be the first orbital telescope using Si meta-shell optics and the first instrument to use CAT gratings and laterally graded ML mirrors in space. These technologies have been matured in the lab to TRL 5-6 as part of development for missions like Arcus or Lynx. *PiSoX* will provide invaluable flight experience for these technologies, yet can be executed with minimal risk given the significant prior investments by NASA.

The dispersion of the gratings is matched to the lateral grading of the ML mirror set at $45°$ to the optical axis. By smoothly rotating the instrument about the optical axis through $180°$, we can measure the three Stokes parameters I, Q, and U across the entire band and discern wavelengths with a spectral resolution $\lambda/\delta\lambda \approx 100$.

The spacecraft will be provided by NanoAvionics with flight-proven components. *PiSoX* is designed for the ESPA Grande rideshare to a low Earth orbit with modest inclination. We have a 1 year observing plan that will satisfy the science goals, achieving minimum detectable polarizations (MDPs) of 3-10% for over a dozen targets.

PiSoX is a mission to examine neutron star atmospheres and magnetospheres and the jets and disks of active galaxies – key 2010 Decadal Survey topics. *PiSoX* leverages several new but highly developed, now low-risk technologies with a team that advances the readiness of early-career researchers and students to assume roles in advancing NASA's strategic objectives.

1. SCIENCE OBJECTIVES

Polarimetry provides two extra dimensions that have been underutilized in astronomy. If included, it can elucidate the underlying physics and geometry of the emission region much better than non-polarimetric observations. Generally, light can be polarized when it is emitted in or passes through areas with strong magnetic fields or scatters, e.g. off electrons in accretion disk atmospheres. There are many examples of the value of optical and radio polarimetry such as finding hidden broad line regions in quasars,[2] demonstrating that jets and supernova remnants accelerate electrons to very high energies,[3,4] and examining the emission regions of pulsar magnetospheres.[5]

1.1 Magnetized Atmospheres of Neutron Stars (NSs) and Pulsars

Some of the strongest magnetic fields in the universe are observed in isolated NSs, making them unique laboratories for the interaction of matter and fields, as well as for testing quantum electrodynamics (QED) effects.[6] *PiSoX*, can be used to sample a large range of NS B-fields with different targets to understand the origin of atmospheric absorption lines, verify QED predictions, test atmosphere models, and assess effects in pulsar magnetospheres. Recently, atmosphere modeling generally includes linear polarization but this aspect of the models cannot be tested currently. These models are needed in order to accurately determine a NS radius, R, that is key to testing equations of state of matter at nuclear densities.[6–8] *PiSoX* will provide the missing polarimetry information needed to test these atmosphere models (see Fig. 1). *IXPE* will observe NSs to examine magnetospheric phenomena and the effects of QED on the pulsed radiation but the NS surfaces are observable only below 1 keV, which makes these measurements impossible for *IXPE* but perfect for *PiSoX*.

Furthermore, identifying an atmospheric absorption feature by observing the polarization across the feature would provide the gravitational redshift at the NS surface, $z = (1 - 2GM/[Rc^2])^{-1/2} - 1$, giving the NS mass M when R is determined from atmosphere fitting. Measuring z this way has never been done for any NS (although claimed[9] but not confirmed[10]), so *PiSoX* provides a ground-breaking opportunity. Determining both M and R for any NS is critical if we ever hope to use NSs to study the fundamental nature of matter itself. As listed in Table 1, several of the candidate targets have absorption features in their phase-averaged 0.25-0.5 keV spectra that are thought to arise from proton cyclotron features when $B \gtrsim 10^{13}$ G[11–13] or gravitationally redshifted O VIII.[14] The centroid of a deep absorption feature in RX J1308.6+2127 varied with pulse phase, perhaps due to a multipolar magnetic field.[13] As the lines appear to be resolved with FWHM of ~ 150 eV level,[11,13] we require a spectral resolution of better than 50 eV in order to measure the polarization change through the line, as predicted in atmosphere models (Fig. 1 right;[8,15]). To resolve these lines requires splitting the spectrum into 4-10 bands, requiring spectrally integrated MDPs of $\leq 10\%$ in order to yield MDPs of $\leq 30\%$ per band.

Even without absorption features, the polarization fraction and position angle (PA) vary with energy within the *PiSoX* band in a manner that depends on the atmosphere's composition and whether the atmosphere is
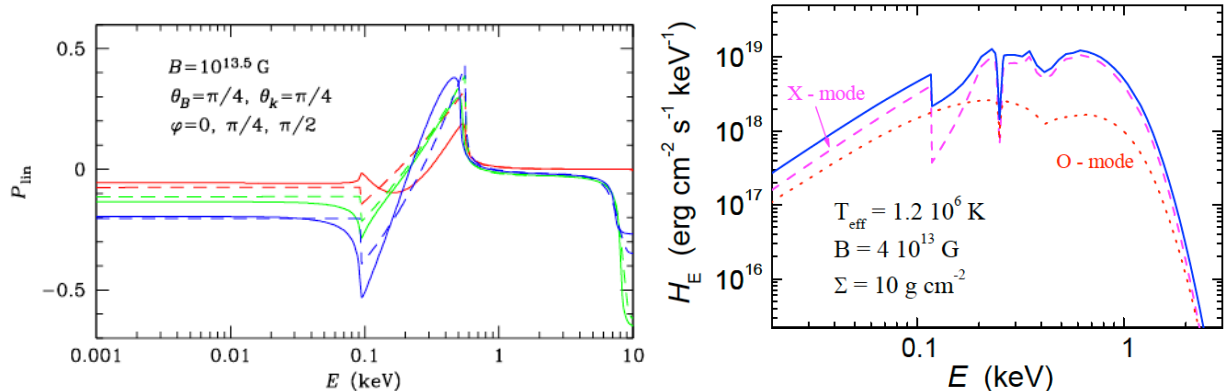
Figure 1. *Left:* Models of the polarization fraction, given as the intensity-normalized Stokes Q, and its variation with energy for a magnetized Fe atmosphere with $B = 10^{13.5}$ G.[16] (Dashed lines are analytical approximations.) The values in the legend represent the angle of the field relative to the surface normal, θ_B, the polar and azimuthal angles of photon propagation relative to the surface normal, θ_k and φ. The angle φ can be determined from the soft X-ray polarization variation with E, measurable with *PiSoX*. *Right:* Model of an atmosphere showing how the emission lines appear differently in different polarizations, given by the extraordinary (X) and ordinary (O) modes of photon propagation relative to the local magnetic field.[8]

gaseous, liquid or solid (Fig. 1 left,[16]). At these high magnetic fields, the vacuum is birefringent,[17, 18] polarizing the X-rays from the surface up to 80%[19] for a gaseous atmosphere and 20-50% for a condensed surface. To temporally resolve the variations requires MDP < 30% in 10 pulse phase bins, or a pulse averaged MDP of $\leq$ 10%. With periods in the 3-20 s range,[20] we require X-ray time-tagging to < 0.1 s.

PSR B0656+14, and Her X-1 are more "traditional" pulsars with $B \sim 10^{12}$ G. An observation of PSR B0656+14 could distinguish between fan and pencil beam models of magnetospheric emission via rotation of polarization angle ϕ with pulse phase and constrain NS spin axis inclination and B-field obliquity.[21] Pulsars will be observed by *IXPE* but the X-ray emission of PSR B0656+14 peaks near 0.3 keV and is too faint above 2 keV for *IXPE*. While most models assume that B is dipolar, rapid changes of the polarization angle (PA) would indicate that field multipoles are important near the surface. The sub-keV pulsed emission of Her X-1 does not come from the surface or polar cap, as its effective size is much larger than the NS, and is more likely from the inner edge of the warped, highly inclined accretion disk where the magnetosphere disrupts it.[22] Two scenarios can only be distinguished using *PiSoX*: Either the beamed hard X-rays heat a spot on the disk, creating a scattering atmosphere up to 11% polarized[23] or the sweeping magnetic field heats the ionized disk and the radiation is predominantly synchrotron, up to 70% polarized if the field is very ordered there. Either way, the polarization PA would vary significantly with pulse phase and would probe the state and geometry of the transition region where material flows from the disk into the accretion column. Short *PiSoX* observations would easily detect polarization even in the case of a disk scattering atmosphere.

1.2 Soft X-rays from Active Galactic Nuclei (AGN)

The soft X-ray emission of active galaxies can result from several different mechanisms that can be distinguished with observations by *PiSoX*, ranging from strongly magnetized jets to mildly polarized accretion disk atmospheres and coronae that current observations cannot discriminate. The soft spectral components of these sources makes *PiSoX* an excellent instrument for exploring models of the soft X-ray emission.

1.2.1 Relativistic Jets from Blazars

Blazars, which include BL Lac objects and highly variable quasars, contain parsec-scale jets with $\beta \equiv v/c \sim 0.98$ or higher. Blazar jets are among the most powerful outflows in the universe. While the jet launching mechanism is not completely understood, it is clear that magnetic fields must be involved via the Blandford-Payne or Blandford-Znajek mechanisms.[4] Their X-ray spectra are often quite steep – power law spectra with spectral energy indices $\alpha = 1.5 - 2$. With *PiSoX*, we will measure the uniformity and orientation of the magnetic field in blazar jets to constrain their origin and evolution.

In the so-called high synchrotron peak blazars (HSPs such as Mk 421), the X-ray spectrum is most likely synchrotron radiation from high energy electrons. If the soft X-ray polarization is much less than ~70%, then models with simple, uniformly magnetized X-ray emission regions will be ruled out. Jet and shock models predict different B-field directions and, consequently, PA. For knots in a laminar jet flow, B can be nearly parallel to the jet axis,[24, 25] while for shocks B should be perpendicular.[26] Both cases were observed in the optical and radio polarimetry of the M 87 jet,[27, 28] indicating highly ordered magnetic fields in regions that also produce X-ray emission.[29] To allow for low ordering as observed in the UV for some HSPs, we require MDPs ≤ 10%.

In low synchrotron peak blazars (LSPs such as 3C 273), the emission above 2 keV is thought to be dominated by inverse Compton (iC) emission or X-ray reflection from an accretion disk. Notably, 3C 273 has a separate spectral component that dominates below 1 keV, whose polarization cannot be examined by *IXPE*. If it is synchrotron emission, related to the superluminal jet in the core, then the soft X-rays will be more highly polarized than the hard X-ray emission – up to 70%. If, instead, it is related to the accretion disk, then the polarization would be below 10%. An MDP of 10% should discriminate these cases.

1.2.2 AGN Soft Excesses

Some AGN, such as the subclass known as narrow line Seyfert 1s (NLS1s),[30] have an X-ray spectral component below 1 keV – a soft X-ray excess over a power law component that dominates the spectrum above 2 keV.[31] The flatter power law that dominates the 2-10 keV band is most often modeled as reflection of X-rays from a hot corona off of an accretion disk,[32, 33] and its polarization properties are observable by *IXPE*. The polarizations of soft excesses, however, would only be measurable by *PiSoX*.

There has been a significant debate in the past few decades regarding the nature of these soft excesses. They have been variously modeled as a black body,[31] a steep power law with $\alpha = 1 - 2$,[34, 35] relativistically smeared absorption above 0.6 keV,[36] or as a collection of relativistically broadened emission lines such as L shell transitions of Fe.[37] Tidal disruption events (TDEs) have X-ray spectra that are very similar to those of NLS1s but are transient, probably triggered when a star breaks up after a passage close by a supermassive black hole but are otherwise inactive.[38]

The thermal and emission line models would have coronal or disk-like geometries, with polarizations ≤10%. There is growing evidence from rapid variability,[39] radio imaging[40] that NLS1s and some TDEs[41, 42] have pc-scale relativistic jets in their cores, linking them to blazars. Several NLS1s show evidence of collimated outflows contributing to the X-ray emission.[30, 43] A detection of >10% polarization would favor a jet model of the soft excess, linking these sources to blazars and rule out thermal and coronal models. RE J1034+396 is an interesting case with a 3550 s quasi-periodic oscillation.[44]

1.3 Polarization metrics

The MDP is the lowest level of polarization that we can distinguish from random noise at the 99% confidence level. For an instrument with modulation factor μ, MDP = $4.29/(\mu RT^{1/2})(R + B)^{1/2}$,[45] where μ is the ratio of the polarization-modulated signal to the average, R is the source count rate, T is the exposure time, and B is the background rate. When B is small, as it is for our design (§ 2.6.3), then MDP = $4.29/(\mu[RT]^{1/2})$, so for a given exposure time and source flux density MDP $\propto 1/(\mu\mathcal{A}^{1/2})$, where $\mathcal{A} \equiv \int Ad\lambda$ is sometimes referred to as the integrated area of the system. While MDP is a good indicator of instrument sensitivity, source modeling requires good *measurements* of polarization, not just detections. Thus, MDPs should be below the expected polarization fractions by ×2-3.

Sometimes PAs can be estimated from external data. Then, the fractional polarization can be estimated, as was done effectively in POGO+ observations of Cyg X-1 to constrain the lamppost model of the accretion disk corona.[46] In such a case, the uncertainty in the polarization fraction is $\sigma_P = 1/[\mu(0.5RT)^{1/2}] \approx$ MDP/3 or 2-3% for most of our observations.

Table 1. Preliminary Observing Plan[a]

Category	Name	Time (Ms)	MDP (%)	Notes
Solo NSs	RX J1856.5−3754	1.0	8	Brightest isolated neutron star
	RX J0720.4−3125	1.0	10	Absorption line at 293 eV[11,14]
	RX J1605.3+3249	1.5	9	Absorption line at 403 eV[14]
	RX J1308.6+2127	1.0	10	Abs'n line varies: 107-256 eV[13,14]
XRB Pulsar	Her X-1	0.3	3	Magnetosphere-disk interaction
Solo Pulsar	PSR B0656+14	1.0	7	Magnetospheric emission
AGN	Mk 421	0.1	3	Bright high spectral peak (HSP) blazar
	1H1426	0.5	5	HSP blazar
	Mk 501	0.5	5	HSP blazar
	3C 273	2.0	10	Low spectral peak blazar, soft excess
	RE J1034+396	1.0	8	Narrow Line Sy 1 (NLS1)
	Ark 564	1.0	8	NLS1
	TBD	1.0	5	Tidal Disruption Event (TOO)
Null	Capella	1.0	4	Null polarization target

[a]We assume 40% observing efficiency. The blazars can be highly variable and may require substitution.

NASA's Strategic Objective: Understand The Sun, Earth, Solar System, And Universe

Science Goal	Science Objective	Measurement Objective	Measurement Requirement	Instrument/Mission Requirements
Understand the fundamental principles of physics in our universe through the study of compact objects	Study the nature of soft X-ray emission from Active Galactic Nuclei	Measure the polarization position angle (PA)	$\sigma_{PA} \leq 5°$	• 180˚ roll capability • Pointing stability < 6" (1 σ) • $AT > 8e6$ cm² Å s
		Measure the fractional polarization (P)	$\sigma_P \leq 3\%$ (MDP = 10%)	
		Observe a Tidal Disruption Event during outburst	Obtain MDP = 10% within 4 weeks of outburst	• TOO response < 1 week • $\mathcal{A} > 4$ cm² Å
		Sample enough AGN and blazars to examine differences	Observe at least 3 targets	Mission Lifetime > (2 cm² Å)/$\mathcal{A}$ yr
	Probe the magnetic fields and atmospheres of neutron stars and identify absorption lines	Measure the PA and FP as a function of phase	$\sigma_{PA} \leq 5°$, $\sigma_P \leq 10\%$ for 0.1 phase of 1s pulsar (MDP = 30% per bin, total MDP = 10%)	Same as for PA, P requirements for AGN; time-tag events to < 0.1s (0.1 x phase for 1 s pulsar)
		Measure the PA and FP as a function of energy	Same as for phase but in 50 eV bins	Same as for PA, P requirements for blazars; dE < 50 eV
		Sample sources with different absorption line energies	Observe at least 3 targets	Mission Lifetime > (2 cm² Å)/$\mathcal{A}$ yr

Figure 2. *PiSoX* science traceability matrix. T is a target exposure time and $\mathcal{A}$ is the integrated area of the instrument (§1.3). The minimum mission requires ≥ 3 targets in both categories of source, requiring a mission lifetime $\geq (4$ cm² Å)/[a] yr; we have 100% margin with $\mathcal{A} = 8.3$ cm² Å (§2.6.5) and a 1 year mission.

1.4 Observing Plan

A preliminary observing plan for a 1 year mission is given in table 1 for an instrument with $\mathcal{A} = 8$ cm²Å, achievable with our design (§ 2.6.5). The plan includes 6 targets in each of our primary categories: neutron stars and AGN with soft spectra. Due to the difficulty of developing conclusions about an entire class of source from one or two targets, the "minimum mission" we consider scientifically useful is to obtain > 10% MDP for each of 3 sources from both of our two categories. This criterion sets the instrument requirements (Fig. 2). Published spectra for these sources were used to compute count rates in the *PiSoX* instrument. In addition to the science targets is a "null" calibrator – a bright, unresolved binary of cool stars with thermal coronae. The table does not include the many other sources that may be polarized and are comparably bright to the primary targets. These secondary targets include magnetic dwarf novae, nearby Galactic X-ray binaries in outburst and other AGN that may be of interest to guest observers after the first year of operation.
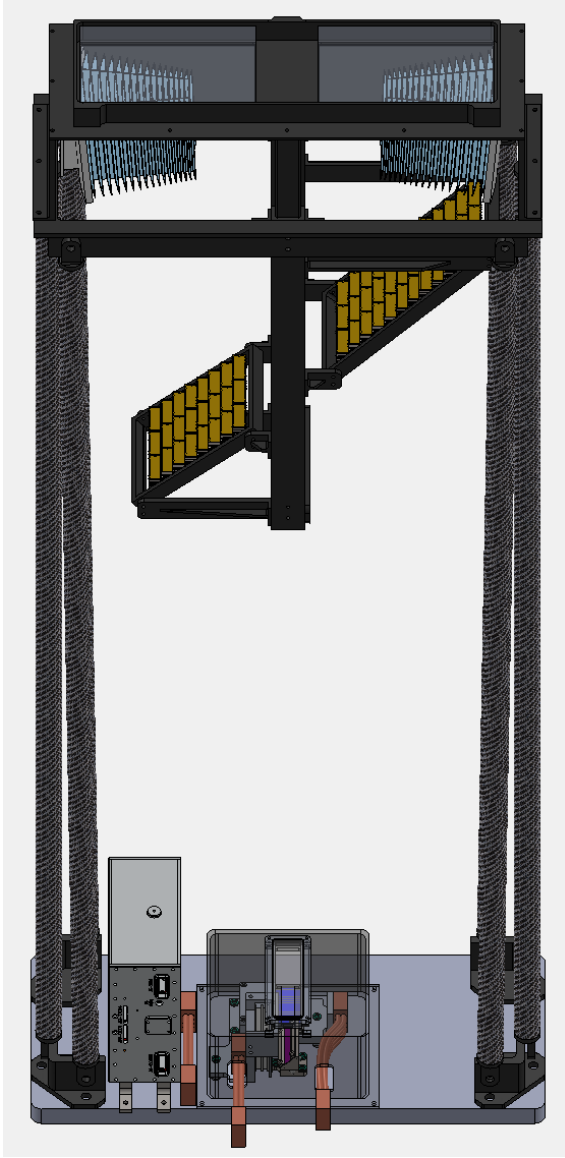
Figure 3. Cutaway rendering of the configuration for the *PiSoX* instrument. It is about 1.25 m tall, and has Si mirrors made of curved and polished segments about 100 mm tall, as developed by GSFC (colored light blue). The optics section is 400 mm wide, 400 mm tall, and 100 mm deep, including the gratings (colored gold). The orientation of the grating bars is parallel to the long dimension of the aperture and gratings are blazed so that they disperse a focused spectrum at the laterally graded multilayer mirror (LGML, magenta) inside the detector housing, better shown in Fig. 4. The detector housing is shown as a translucent box but is designed to be light-tight with optical blocking filters. Only the imaging CCD detector (dark blue) is visible in this rendering. Thermal straps (copper) connect to the heat dissipation system of the spacecraft. Flexprints (not shown) connect the two detectors in the detector housing to the tall box containing the digital and analog electronics for driving the CCDs and finding events. There is only one polarization channel, so the instrument has to be rotated through 180° during observations. More details of the optics section and the focal plane are shown in Fig. 4. The payload $+z$ axis is along the optical axis, with the origin at the imaging detector, and $+x$ is toward and along the LGML.

2. PAYLOAD DESIGN

The science instrument leverages previous funding various grants to make focusing optics, multilayers, gratings, and CCDs. Together, these high technical readiness level (TRL) technologies enable us to build *PiSoX* with minimal risk. Schematically, the design is the same as for the *REDSoX* Polarimeter.[47] Here, we outline various modifications for *PiSoX*.

2.1 Focusing Optics

The *PiSoX* mirrors are based on the Si metashell optics developed by the Goddard Space Flight Center (GSFC) group under the direction of Dr. William Zhang.[48] The GSFC group is currently using this technique to fabricate a Wolter I mirror assembly for a sounding rocket payload, OGRE (Off-plane Grating Rocket Experiment,[49]) led by Prof. Randall McEntaffer (PSU). The point spread function (PSF) of the mirror assembly will have a half-power diameter (HPD) of $\lesssim 5''$. The mirror assembly that will result from this work will easily meet the science and spaceflight requirements of *PiSoX* and will have been tested before work on our optics would begin.
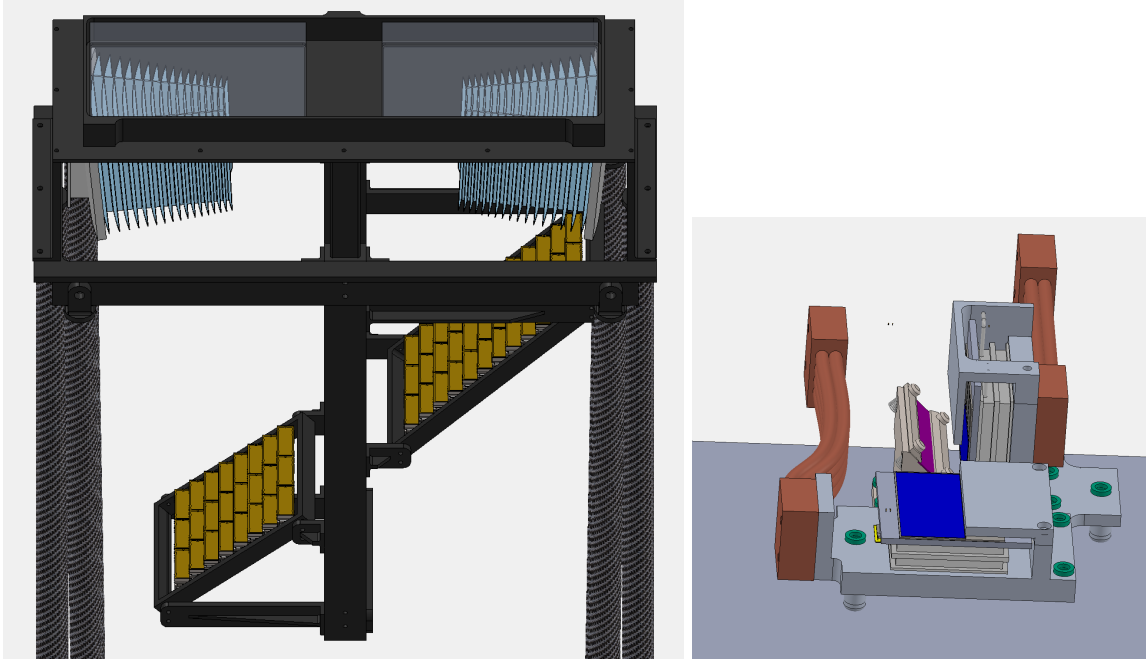
Figure 4. *Left:* View of *PiSoX* optics section. Thin Si mirrors (light blue) provide focusing. The gratings (gold) are stair-stepped to match the Bragg condition at the multilayer mirror (see §2.2[47]). *Right:* Focal plane layout without the enclosing housing. The imaging CCD (dark blue) is at the direct focus while the LGML (magenta) is at the spectrometer focus and reflects to the vertically oriented polarimetry detector (dark blue). Copper straps connect the CCD TECs to the spacecraft's cooling system.

For *PiSoX*, sources are only measurable when on axis, so off-axis imaging quality is irrelevant. Therefore, we baseline a purely parabolic, single-bounce design for *PiSoX* mirrors, eliminating hyperbolic secondaries. A single bounce mirror system requires half of the mirror segments and less alignment work for a given effective area, making the mirror system simpler, substantially less expensive, and much lighter than a Wolter I design with the same geometric collecting area. With Ni coating, reflectivities average 70% for the graze angles between 3 and 10°, giving a total effective area of 130 cm^2 that is independent of energy in the 0.2-0.4 keV band.

Because pure parabolic mirror systems are not common in X-ray astronomy, we have studied the optical properties of the images by raytracing. We used the Interactive RayTrace (IRT) code for IDL provided to MIT by Prof. Webster Cash (Colo. Univ.) for the *Chandra* project to make spot diagrams, compute HPDs, investigate off-axis aberrations, etc. The telescope length, measured from the entrance aperture to the imaging (and spectroscopy) focal plane is limited to be no longer than 1.19 m due to the spatial limitations of the ESPA Grande rideshare payload (see § 3.1). We will refer to this length as the focal length of the system.

The spectral resolution of a transmission grating spectrometer is determined by the size of a point source's image along the dispersion. Thus, only the 1D FWHM of the image is critical to the performance. We find that azimuthally symmetric mirrors with a half-power diameter (HPD) of ≲10″ meet our requirements when sectored. We use ±18° sectors of mirror shells (Fig. 4), on opposite sides of the optical axis to reduce the telescope 2D PSF from 10″ HPD to 2.9″ in 1D (FWHM) for use in spectroscopy,[50] projecting to $\delta x = 17\mu m$ along the dispersion. For a grating spectrometer, $R = \lambda/(\delta\lambda) = x/(\delta x)$; $x = 11.4 - 35$ mm is the dispersion distance for the gratings in our design (§ 2.2) and the baseline wavelength range of 30-65 Å. At these dispersion distances, R is in the range 680 to 2000, a factor of 7-20 better than the requirement.

2.2 Gratings

As with the *REDSoX* Polarimeter, we baseline Critical Angle Transmission (CAT) gratings[51] developed in the Space Nanotechnology Lab (SNL) at MIT. CAT gratings can be reliably produced in a 10×30 mm format.[52,53] Over a dozen CAT gratings of 200 nm period and 4 μm membrane thickness have been tested in the MIT

polarimetry beamline, including several in a 27 mm square format fabricated as part of *Arcus*[54] phase A development. Efficiencies of 20% are achieved in lab measurements in first order as needed for *PiSoX* (Garner, et al. in prep.). Alignment is performed at the mount and assembly level, as described in § 2.6.2, based on a method prototyped for *Arcus*.[55] This method has been shown to align gratings to a single reference to within the tolerances given in Table 3, which are based on analysis and raytracing.

Precise positioning of the gratings is given in our paper[47] that includes raytrace validation. For *PiSoX*, there are 8 rows of 3 gratings each in the lower sector and 12 rows of 3 each in the upper sector for a total of 60 gratings. Including 15% blockage by the gratings internal L1 and L2 support structure and 20% blockage by the grating assembly framework, the average transmission into +1 order is 11.6% across the *PiSoX* band at the optimal blaze angle of 0.8°.

2.3 Laterally Graded Multilayer Mirrors (LGMLs)

LGMLs have been made by Eric Gullikson at the Lawrence Berkeley National Lab (LBNL) Center for X-ray Optics that are suitable for our design. The $Cr/B_4C/Sc$ layer combination has a reflectivity over 7% between 31 and 70 Å based on measurements at the Advanced Light Source at LBNL.[56,57]

2.4 CCD Detectors

The CCD detectors for PiSoX are designed and fabricated by the MIT Lincoln Laboratory (MITLL), which has provided CCD imaging detectors for X-ray missions dating back more than 25 years and including ASCA, *Chandra*, and Suzaku. The two CCID-94 devices to fly on PiSoX are backside-illuminated (BI), 50 mm ×25 mm (2048×1024-pixel) frame-store CCDs that are equivalent to two side-by-side Suzaku CCID-41 devices, with 24-μm pixels. They trace direct heritage from the Suzaku BI CCD that performed exceptionally well for the nearly 10-year mission lifetime in a low-Earth, high-inclination orbit that regularly traversed the South Atlantic Anomaly, with features including a 3-phase polysilicon gate structure, low noise (<4 e$^-$) readout amplifiers, and charge injection.

One CCD will be used to record the dispersed, polarization-sensitive spectrum reflected by the LGML, and the second will record the zeroth-order source image to ensure proper acquisition of the target and monitor its broad-band flux, giving us a redundant measurement of Stokes I. Each CCD will be read out at 625 kHz through 8 parallel PJFET outputs, for a frame integration time of 1 s. The polarization detector will additionally have a "parallel sum" mode in which the imaging area is continuously read out and multiple rows are summed on-chip to provide time resolution of better than 100 ms to allow phase-dependent analysis for pulsars with periods of > 1 s. For this reason, the dispersion direction is perpendicular to the CCD parallel transfer direction, and the dispersed spectrum will fit comfortably within the 50 mm width of the detector.

The CCD spectral resolution requirements are modest, with FWHM < 100 eV required to reduce background and to separate 0.2 keV photons from 0.4 keV photons from overlapping orders in the dispersed spectrum. This requirement plus the use of charge injection and short frame time allow operation at -50C with minimal dark current or CTI effects. This temperature will be controlled to $\pm$1C by one 2-stage thermo-electric cooler (TEC) on each CCD, removing heat to the spacecraft hot side via thermal straps. These high-heritage TECs are manufactured by II-VI Marlow, which fabricated similar TECs for Suzaku that worked flawlessly over the course of the 10-year mission.

Each CCD is coated with 50 nm of Al to block optical light, and the entire focal plane including the LGML is contained within a light-tight detector housing to further eliminate optical contamination from the bright Earth limb. The entrance aperture for the LGML and zeroth-order CCD is covered by a 50-nm Al + 50-nm polyimide filter mounted on a 95% transparent metal mesh, manufactured by Luxel, which has provided similar filters for missions such as Chandra and Suzaku. This contamination blocking filter is kept warm (0–20C) with a heater to prevent molecular contamination from building up on the cold CCD surfaces or accumulating along other optical elements and reducing the soft X-ray response. The combined CCD QE and filter transmission is expected to be about 10% at 0.2 keV and 50% at 0.4 keV.

Subsystem	Mass (kg)
Door Assembly	5.5
Mirror Assembly	7.4
Grating Assembly	3.4
Focal Plane	2.2
Electrical Box	4.3
Optical Bench	7.3
Total	30.1

Table 2. Payload Component Masses. With 25% margin, the total mass is 37.6 kg. The focal plane includes two CCDs with associated TECs, the LGML and its mount, the optical blocking filters, thermal straps, and the detector housing.

2.5 Focal Plane Electronics

The focal plane electronics include three electronics boards that drive the CCDs and process the payload data for downlink. The boards and their enclosure are based heavily on those flown on the Regolith X-Ray Imaging Spectrometer (REXIS), an instrument on board the OSIRIS-REx asteroid sample return mission. The REXIS electronics performed nominally over a period of 3.5 years after launch. Two of the boards, the Interface Board and Video Board, comprise the Detector Electronics (DE) and provide power and commanding to the detectors, provide precise clocking signals to the CCDs, and read out, digitize and process the detector signal. The existing REXIS design allows for processing of 16 parallel readout nodes, sufficient for the two 8-node CCDs aboard PiSoX, but will need to be modified to provide active thermal control. The total power draw is expected to be 20 W with 25% margin.

The digitized raw frames are delivered to the third board, the Main Electronics Board (MEB), that includes a Xilinx Virtex 5 FPGA that further processes the raw image frames to greatly reduce the payload data volume. This digital processing follows the method used for over 20 years of X-ray missions, with on-board bias maps employed to identify and measure X-ray events, providing for each event the x and y position, a 3×3 array of pulse heights, and a time counter. Events associated with hot pixels or grades commonly associated with particle interactions can be rejected on-board. After processing, the MEB packages and transfers the event list and exposure information to the spacecraft electronics for downlink. At 166 bits per event and a maximum likely count rate of 50 events per second between the two detectors, the maximum data rate is under 10 kbps. This includes 1 kbps devoted to instrument housekeeping. Occasionally, full CCD frames are needed to diagnose bias maps or an anomaly, requiring a downlink of 25 Mbit per CCD. In this diagnostic mode, consecutive frames need not be telemetered, and the full frame can be stored on-board and downlinked as possible.

2.6 System Considerations and Other Components

This section describes other aspects of the design of *PiSoX*. Table 2 gives the payload component masses.

2.6.1 Structure

PiSoX will use a single-body rigid structure that is as short as possible to fit into the ESPA Grande payload volume (see § 3.1). The payload consists of two major sections. The fore section, the optics module, contains the Si shell mirror assembly and grating assembly. The aft section (the focal plane) contains the detectors, multilayer mirror, and electronics systems. Connecting these two sections are rigid struts made from carbon fiber reinforced polymer (CFRP). Table 3 provides instrument subsystem tolerances relative to the reference frame established by an optical cube on the mirror assembly. Tolerances were determined using analytical formulae verified by raytracing.[47] Mechanical machining and assembly tolerances are sufficient for most aspects of the system. Aligning the gratings and the grating assemblies are carried out on an optical bench and in the MIT X-ray Polarimetry beamline; see sections 2.7.2 and 2.7.3 for details.

2.6.2 Attitude Control and Alignment

Based on optics ray tracing, if pointing jitter is $\gtrsim 20''$ (3σ), light would be lost as the dispersed spectrum is displaced from the Bragg peak of the LGML along the dispersion, in a manner comparable to PSF broadening. Therefore, we require that the spacecraft attitude determination control system (ADCS) hold the orientation of the telescope's boresight to about $6''$ (1σ). In order to change the position angles of the LGML mirrors with

Table 3. Instrument subsystem tolerances (1 σ)

Subsystem	Positional (mm)			Angular (′)		
	x	y	z	x	y	z
Grating assembly	1.0	1.0	1.0	6.0	6.0	60
CAT grating in assembly	1.0	1.0	2.5	60	6.0	60
ML mirror	0.1	1.0	1.0	1	60	6.0
Imaging CCD	2.0	5.0	0.1	120	120	120
Polarimetry CCD	5.0	2.0	5.0	120	120	120

Tolerances are relative to a reference cube on the mirror assembly. Tolerances in green indicate those satisfied by machining and assembly accuracies to better than 0.1 mm; others will be achieved during alignment tests at MIT (§2.7.3). The coordinate system is defined in Fig. 3.
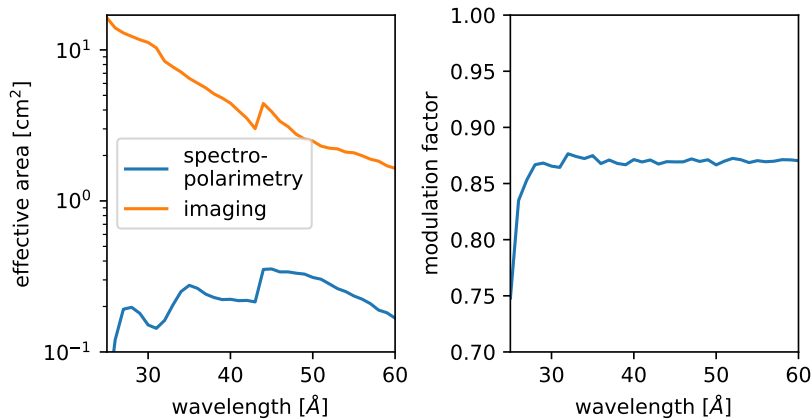
Figure 5. *Left:* Effective area of the system based on raytracing and confirmed by analysis. *Right:* Modulation factor, averaging about 87%.

respect to the sky, the spacecraft roll angle will be varied to span a range of 180° by continuously rotating or stepping at periodic intervals through the observation. Due to possible source variability on time scales of 10 ks, the satellite should complete a 180° scan at least once every 5000 s. In order to accurately assign the roll angle to any given X-ray event, the scan rate should be no faster than 1°/s and the roll angle and should be accurate to 1° every second during data collection. The initial roll angle for any given observation is arbitrary. See § 3.1 for more details about the attitude system.

2.6.3 Sources of Background

From the Suzaku mission (600 km altitude and 31° inclination), the particle background in the backside-illuminated CCD was 5×10^{-8} cnt/s/keV/pixel, or 1.5×10^{-5} cnt/s/mm^2 in a 0.2 keV band at 0.3 keV.[58] In the cross dispersion direction, the dispersed spectra extraction region will be about 3 mm tall due to the 20° beam divergence from the LGML, which is located at the spectroscopic focus. In the dispersion direction, the spectra are 20 mm long giving a total of 60 mm^2 for the extraction region. For an exposure of 10^6 s, we expect 900 counts from particles, while obtaining an MDP of 10% requires about 2,500 counts, so particle background is minor but included in our MDP estimates in any case. The X-ray background in the *PiSoX* bandpass is dominated by Galactic emission. A full ray-trace simulation including in particular gratings and the multi-layer mirror using the marxs code[47,59] show that off-axis X-rays are dispersed in such a way that their reflection is suppressed by the ML, in contrast to on-axis photons which are diffracted such that they hit the Bragg-peak. Using a measured flux for the Galactic emission and background AGN,[60] the ray-trace predicts an X-ray background rate of 2 counts per 1 Ms – clearly negligible.

2.6.4 Payload Technical Readiness Levels

Si metashell optics are under fabrication at GSFC with APRA funding. The entire process of cutting Si blocks, mounting into modules, and then integrating into an assembly will have TRL = 6 by Fall 2021. Gratings have

already been fabricated and tested that meet our specifications, but assembly requires alignment that is currently in the validation process using internal MIT funding.

As part of our current APRA grant to demonstrate technology for soft X-ray polarimetry, MIT is acquiring a simple module of Si shell optics from GSFC to focus the X-rays from our electron impact source within the MIT X-ray Polarimetry beamline (see § 2.7). We expect to install the optics module in the beamline in the fall of 2021. Thus, we will be able to complete an end-to-end test of the polarimeter design with all essential components on rotational or translation stages as needed: a 100% polarized source, focusing optics, an internally aligned grating assembly, a multilayer mirror, and the current lab CCD detector, raising the TRL of the integrated system to 6.

2.6.5 Baseline Performance

Using detailed analytical models of the reflectivity and QE curves and raytracing, we obtain $\mathcal{A} = 8.3$ cm^{2}Å, consistent with the 1 year science plan (§ 1.4). The minimum mission (§ 1.4) would still be possible if the overall performance is degraded to $\mathcal{A} = 4$ cm^{2}Å, giving us about 108% margin. One may also estimate $\mathcal{A}$ by $A\ T_g\eta\ r\ Q\ \Delta\lambda$, where $A = 130$ cm^2 is the mirror effective area, $T_g = 0.116$ is the average grating efficiency including obscuration by supports, $r = 0.07$ is the average reflectivity of the LGML, $Q = 0.33$ is the average QE of the detector (including the filter), and $\Delta\lambda = 30$Å is the bandwidth of the system. The factor η is due to the combined effects of the optics broadening, attitude variation, event centroiding, and structural variation during observations that cause losses due to Bragg peak mismatch that we find to be no more than 30% ($\eta = 0.7$) based on raytracing. This rough estimate gives $\mathcal{A} = 7.3$ cm^{2}Å, within 15% of our detailed calculations. The imaging detector provides an independent, simultaneous measurement of I in the 0.2-0.4 keV band (and up to 10 keV), with $\mathcal{A}_0 = 250$ cm^{2}Å for zeroth order grating efficiencies of about 20%. The zeroth order count rates for our targets are 0.2-20 cnt/s.

2.7 Integration and Testing

Integration and test of the instrument will be the responsibility of the MIT payload team and will take place at MIT. Subsystem testing, instrument integration, alignment and performance testing will occur at MIT using the MIT X-ray Polarimetry Laboratory beamline. Environmental testing, including launch vibe and thermal vacuum testing, will take place at MITLL. A high-level view of the integration and test plan is shown in Figure 6. The plan consists of three main sections: component testing, subsystem testing and integrated instrument tests. Component-level testing of the mirror assembly and LGML will take place at GSFC and LBNL respectively, prior to delivery to MIT. The gratings and the CCDs will be tested at MIT prior to subsystem integration. At MIT, the gratings and the mirror assemblies are integrated into the optics module, and the CCDs and LGML are combined to form the focal plane. Both of these subassemblies are tested separately, and then together at MIT in the Polarimetry beamline. To complete instrument integration, the optics module and focal plane are assembled into the instrument structure. Integrated alignment and performance testing is then conducted in the MIT beamline. The instrument is then transported to MITLL for environmental testing, including vibration tests and thermal vacuum cycling and balance. Upon the completion of environmental testing the instrument is returned to MIT for a final alignment and performance check in the X-ray beamline before delivery for integration with the spacecraft.

2.7.1 MIT Facility

The MIT X-ray Polarimetry beamline is an 11m long X-ray beamline that is extendable to 17m. It was originally designed and constructed to test the *Chandra* high energy transmission gratings. It has since been adapted to produce polarized light at several energies in order to test components for soft X-ray polarimetry applications and is described elsewhere.[56, 57, 61–63] Using the beamline, we will be able to separately test each component of *PiSoX*, from optics through the focal plane. Furthermore, we can test combinations of components such as the optics module, which is a combination of the mirror and grating assemblies, and the focal plane, which has both flight CCDs and the LGML. Finally, the assembled payload will fit into the 1.3m diameter chamber to complete the performance and alignment testing.
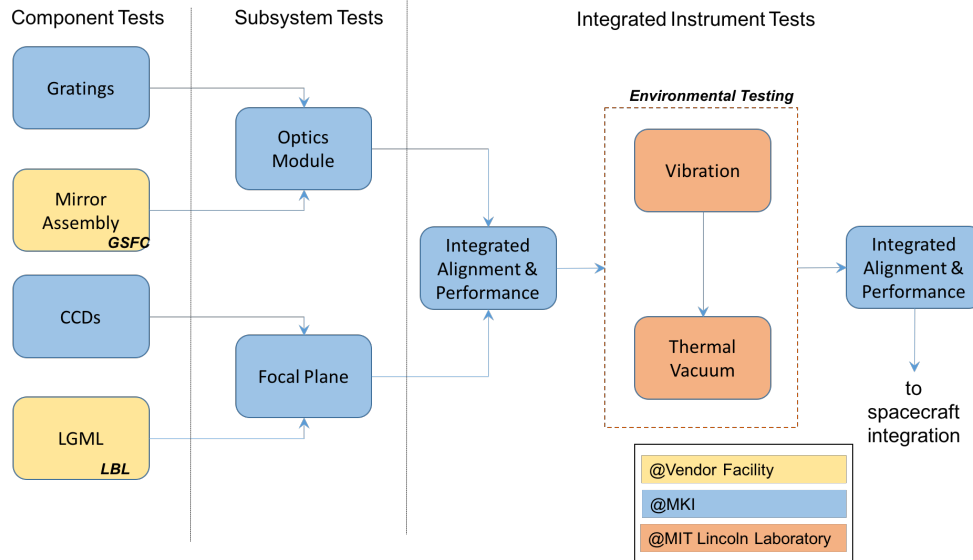
Figure 6. Block diagram of instrument-level integration and test. GSFC and LBNL testing involve X-ray testing, as do all the MIT tests shown here. The plan shows that all stages of development can be verified. Both the MIT and LBNL facilities use polarized X-ray sources.

2.7.2 Component Testing: Gratings

Testing of the performance and alignment of the CAT gratings is critical to *PiSoX* and our team has the facilities and experience to do both. The performance and quality of the gratings will be measured and verified in our X-ray beamline. These measurements have been performed before with similar CAT gratings, in particular using the prototype gratings for the Arcus mission (Garner, et al., these proceedings).

CAT grating alignment procedures have been developed and demonstrated as part of Arcus phase A work.[53,55] With an MIT internal grant, we have built a grating alignment system modeled after this tool, built and tested for CAT grating testing but customized for this project. This technique uses a UV laser and position-sensitive detectors to measure the reflection and back diffraction off of the CAT grating bars. From that information the orientation and alignment of the gratings can be determined within the tolerances required by *PiSoX* (see §3). An advantage of this method is that it can all be done on an optical bench. Given the number of gratings present in *PiSoX*, this is a huge mitigation to schedule-related risk. Using the laser-alignment tool, the *PiSoX* CAT gratings will be aligned relative to one another as a complete subsystem and to an optical alignment cube mounted to the grating assembly. The alignment will then be checked using the X-ray beamline (§2.7.1).

2.7.3 Subsystem Testing

The *PiSoX* optics module will be aligned and integrated in stages. The grazing-incidence mirror assembly provided by GSFC will arrive as a unit aligned to its own alignment cube. The grating sub-assembly (described in 2.7.2) will then be aligned to the mirror assembly using the alignment cubes of the two subsystems on an optical bench. The MIT Polarimetry beamline can be used to verify alignment in X-rays for both dispersed and 0th order imaging using the facility detector. The shape and size of the images will provide a direct measurement of the alignment when compared to images from raytraces that account for the finite source distance and an incompletely illuminated aperture. The finite source focus is about 130 mm shorter than the telescope length, at 1.06 m from the telescope aperture. A plate with various 25 mm long slits can be scanned across the mirror entrance for fine-grained testing.

The focal plane assembly, with both imaging and polarimetry detectors, requires a determination of the LGML position as mounted on the focal plane with respect to the imaging CCD. ALS measurements provide accurate Bragg peak positions with respect to an LGML edge that will be used as a reference for mechanical assembly and metrology. The positioning can be verified using the MIT X-ray beamline as follows. The LGML
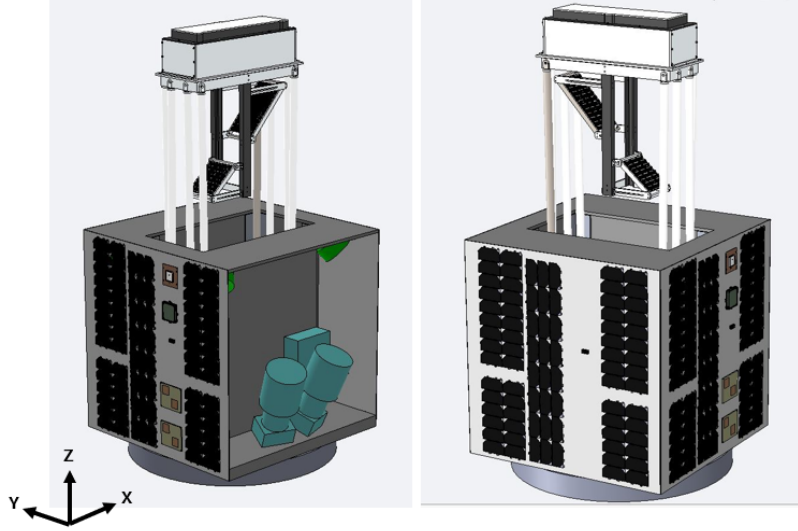
Figure 7. Renderings of the spacecraft with one external radiator panel around the star trackers hidden. Generally, the $+Z$ and $-Y$ faces are in shadow, while $+Y$ and $\pm X$ are used for power generation. In both cases the sheathing and thermal layer around the payload are hidden.

is scanned in a monochromatic beam with a 0.1 mm slit to determine where maximum reflectivity is achieved at 45° to the beamline. By setting the X-ray target to different emission lines, the gradient and the zero point relative to the LGML edge can be confirmed. The stage is then moved by the amount indicated for the zero point and X-ray beam will then illuminate the detector reference point that will provide a match to the Bragg peak for X-rays dispersed by the gratings.

2.7.4 Integrated Instrument Testing

After optics and focal plane subsystem integration, (§2.7.3) the two subsystems can be integrated with the optical bench and tested in the MIT Polarimetry beamline without the facility detector. The focal plane will be out of focus, but we can still use the 0th order image to check for tip and tilt misalignment by comparing to predictions from raytraces. The illumination of the LGML will be out of focus as well but the Bragg condition will be met as long as the distance from the focal plane to the gratings is within the required tolerance (see §3). This will also allow us to test and correct the relative positions of the focal plane and optics by adjusting the optical bench. Critically, this approach allows us to do a full systems test of the payload that is accurate in every way except the distance to the source.

3. SPACECRAFT

3.1 Architecture

The *PiSoX* spacecraft is designed for low Earth orbit (LEO) and will be developed by NanoAvionics. Overviews of the structure and subsystems are provided in Figs. 7. The platform will have subsystems from NanoAvionics and other companies with high heritage in LEO, with a cold-redundant, dual string architecture. The structure will be composed of a 700 mm × 700 mm baseplate, below which the Ruag PAS 610S ESPA ring separation system is mounted. The payload will be centrally mounted on top of this base plate and shear panels will be mounted around the instrument with most of the electronics installed on them.

3.2 Electronics & Power

The flight computer (FC) is the NanoAvionics SatBus 3C2, running the FreeRTOS real time operating system on an ARM 32-bit Cortex M7 CPU with a clock speed of 400 MHz, double-precision floating point unit, 1 MB of internal RAM, 2MB of internal FLASH memory, as well as 3 internal magnetometers. An identical FC is hot-swappable in flight. The FC interfaces to the NanoAvionics Payload Controller (or its backup), which runs Linux, has 256 MB of data storage via microSD cards, and communicates with the payload electronics via TCP/IP.
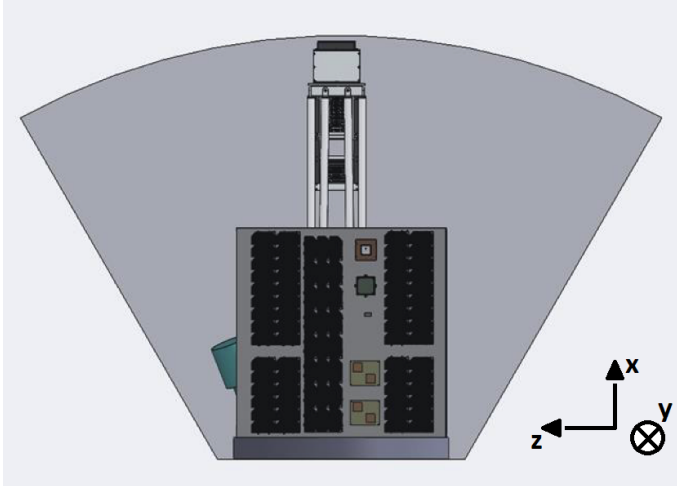
Figure 8. Rendering of the spacecraft in the Starlink rideshare volume. The dimensions of the satellite are $720 \times 735 \times 1400$ mm, within the payload accommodation volume (§4.1). *PiSoX* also conforms to the ESPA Grande payload requirements on mass and center of gravity (§4.1).

3.3 Attitude Control

Attitude knowledge and control is handled by the attitude determination and control system (ADCS) on the spacecraft bus. Components are commercially available with substantial flight heritage. Attitude knowledge and control requirements are $20''$ at $3\,\sigma$ in order to maintain the alignment of the dispersed spectrum and the Bragg peak of the LGML (see §2.6.2). There are two aspects of the attitude control budget: short term variations over seconds to hours and fixed offsets. The former are not correctable in flight so they contribute to the pointing error. The latter will be calibrated out in flight during the commissioning phase of the mission that begins when the telescope door is opened.

3.4 Communications

Three communications channels are available, all with redundant components. A link budget was established for each of UHF, S-Band and X-Band assuming an orbital altitude of 550 km. X-band can be used in ground station tracking mode with a 5m dish for all elevations above $5°$.

4. MISSION IMPLEMENTATION

4.1 Launch Vehicle and Orbit

The mission is designed for operations in LEO for a lifetime of one year. An injection altitude of > 350 km will provide this orbital lifetime for *PiSoX*, which has a mass to area ratio of about 210 km/m², While low inclinations (equatorial orbits) are preferred due to reduced particle background, moderate inclinations are acceptable, such as when launching from Florida. The satellite meets ESPA Grande Payload Rideshare requirements, ($42'' \times 46'' \times 56''$, or $1067 \times 1168 \times 1422$ mm), as can be seen in Figure 8.

The satellite mass estimate is 148.0 kg, including a 10% mass margin on top of 5-10% subsystem mass margin and the 25% mass margin on the instrument. The ESPA interface places an upper mass limit of 465kg on the spacecraft. Thus, we have over 200% mass margin for the ESPA interface. The satellite center of gravity is $16.7''$ from the ESPA ring interface and $0.32''$ from the ring center-line, satisfying the requirements for the ESPA Grande interface to be less than $20''$ from the interface and less than $1''$ from the center-line in both other directions.

4.2 Operations

Given the long exposures, data download is only required once per week via X-band. At the maximum instrument data rate and 40% observing efficiency, a week of data amounts to about 300 MB, easily downloaded in a few minutes via X-band. Operations are based on one S-band uplink per day and one X-band contact per week. Alternatively, data can be downloaded via S-band in 2-3 passes per day. The NanoAvionics Operations Center

(NOC) in Vilnius is responsible for scheduling contacts, uploading commands, and storing downlinked data onto a secure server. Data will then be available for download to the *PiSoX* Science Operations Center (PSOC) at MIT. The PSOC will be responsible for long-term observing plan that is used to create the detailed observing plan on a monthly basis. The PSOC will collect data from the NOC and convert housekeeping and engineering data to physical units for assessing the health of the instrument.

5. TECHNOLOGY DEVELOPMENT

Several systems of *PiSoX* instrument would be flown in orbit for the first time on this mission and are vital to future missions. Thus, *PiSoX* would raise the TRLs of these components (see §2.6.4).

Si metashell mirrors are lightweight and have the potential to provide sub-arcsecond imaging. While Si metashell mirrors are being developed for OGRE, *PiSoX* would provide the first long-term use of these optics in Earth orbit.

CAT gratings are currently planned for Arcus,[53, 54] proposed as a MidEx mission and as an option for Lynx.[53] Arcus will provide high-resolution soft X-ray spectroscopy in the 12-50Å bandpass with sensitivity orders of magnitude higher than any previous astronomical observatory. Lynx is a large X-ray imaging telescope being considered as a flagship mission that would follow on from the successes of *Chandra*.[64, 65]

The CCID-94 detectors (§ 2.4) are a straightforward evolution of the CCID-41 devices flown successfully on Suzaku and have design heritage in *Chandra*, Hete-2 and ASCA. Front-illuminated versions of these devices were successfully fabricated during Arcus[54] Phase A. CCID-94 chips are currently planned for Arcus and Lynx. The *PiSoX* project builds on the development effort for these missions that has been underway at MIT and MITLL for many years.

Laterally graded multilayer mirrors (LGMLs, § 2.3) have never been flown and are the critical polarizing element of our design, which is the only broad-band polarimetry method in the sub-keV band of which we are aware. Just as *IXPE* is an Explorer to measure polarization in the 2-8 keV band, *PiSoX* is a Pioneer of the sub-keV band. The X-ray Polarization Probe (XPP,[66]) would combine larger scale versions of these instruments with a 10-50 keV polarimeter, such as demonstrated by X-Calibur.[67] Thus, XPP would be a general observatory, capable of measuring polarizations across the 0.1-50 keV band simultaneously. Currently funded lab development is focused on extending LGML usage up to 0.8 keV, more thoroughly covering the sub-keV band. See the XPP white paper[66] and the accompanying science white paper[68] for more details.

ACKNOWLEDGMENTS

REFERENCES

[1] O'Dell, S. L., Baldini, L., Bellazzini, R., Costa, E., Elsner, R. F., Kaspi, V. M., Kolodziejczak, J. J., Latronico, L., Marshall, H. L., Matt, G., Mulieri, F., Ramsey, B. D., Romani, R. W., Soffitta, P., Tennant, A. F., Weisskopf, M. C., Allen, D. Z., Amici, F., Antoniak, S., Attina, P., Bachetti, M., Barbanera, M., Baumgartner, W. H., Bladt, J., Bongiorno, S. D., Borotto, F., Brooks, T., Bussinger, S., Bygott, H. K., Cavazzuti, E., Ceccanti, M., Citraro, S., Deininger, W. D., Del Monte, E., Dietz, K. L., Di Lalla, N., Di Persio, G., Donnarumma, I., Erickson, J., Evangelista, Y., Fabiani, S., Ferrazzoli, R., Foster, M., Giusti, M., Gunji, S., Guy, L., Johnson, S., Kalinowski, W., Kelley, A. R., Kilaru, K., Lefevre, C., Maldera, S., Manfreda, A., Marengo, M., Masciarelli, J., McEachen, M., Mereu, P., Minuti, M., Mitchell, M. A., Mitchell, S., Mitsuishi, I., Morbidini, A., Mosti, F., Nasimi, H., Negri, B., Orsini, L., Osborne, D., Pavelitz, S. D., Pentz, C., Perri, M., Pesce-Rollins, M., Peterson, C., Piazzolla, R., Pieraccini, S., Pilia, M., Pinchera, M., Puccetti, S., Ranganathan, J., Read, T., Rubini, A., Santoli, F., Sarra, P., Schindhelm, S., Sciortino, A.,

Seckar, C., Sgrò, C., Smith, B. T., Speegle, C. O., Tamagawa, T., Tardiola, M., Tobia, A., Tortosa, A., Trois, A., Weddendorf, B., Wedmore, J., and Zanetti, D., "The Imaging X-ray Polarimetry Explorer (IXPE): technical overview," in [*SPIE Conference Series,*], *Society of Photo-Optical Instrumentation Engineers (SPIE) Conference Series* **10699**, 106991X (Aug 2018).

[2] Antonucci, R. R. J. and Miller, J. S., "Spectropolarimetry and the nature of NGC 1068," *ApJ,* **297**, 621–632 (Oct. 1985).

[3] Mayer, C. H. and Sloanaker, R. M., "Polarization of the 10-cm radiation from the Crab Nebula and other sources.," *AJ,* **64**, 339 (Jan. 1959).

[4] Blandford, R., Meier, D., and Readhead, A., "Relativistic Jets from Active Galactic Nuclei," *ARA&A,* **57**, 467–509 (Aug 2019).

[5] Radhakrishnan, V., Cooke, D. J., Komesaroff, M. M., and Morris, D., "Evidence in Support of a Rotational Model for the Pulsar PSR 0833-45," *Nature,* **221**, 443–+ (1969).

[6] Harding, A. K. and Lai, D., "Physics of strongly magnetized neutron stars," *Reports on Progress in Physics* **69**, 2631–2708 (Sep 2006).

[7] Ho, W. C. G. and Mori, K., "Modeling Phase-resolved Observations of the Surfaces of Magnetic Neutron Stars," in [*40 Years of Pulsars: Millisecond Pulsars, Magnetars and More*], Bassa, C., Wang, Z., Cumming, A., and Kaspi, V. M., eds., *American Institute of Physics Conference Series* **983**, 340–344 (Feb. 2008).

[8] Suleimanov, V., Hambaryan, V., Potekhin, A. Y., van Adelsberg, M., Neuhäuser, R., and Werner, K., "Radiative properties of highly magnetized isolated neutron star surfaces and approximate treatment of absorption features in their spectra," *A&A,* **522**, A111 (Nov. 2010).

[9] Cottam, J., Paerels, F., and Mendez, M., "Gravitationally redshifted absorption lines in the X-ray burst spectra of a neutron star," *Nature,* **420**, 51–54 (Nov. 2002).

[10] Cottam, J., Paerels, F., Méndez, M., Boirin, L., Lewin, W. H. G., Kuulkers, E., and Miller, J. M., "The Burst Spectra of EXO 0748-676 during a Long 2003 XMM-Newton Observation," *ApJ,* **672**, 504–509 (Jan. 2008).

[11] Haberl, F., Zavlin, V. E., Trümper, J., and Burwitz, V., "A phase-dependent absorption line in the spectrum of the X-ray pulsar RX J0720.4-3125," *A&A,* **419**, 1077–1085 (June 2004).

[12] Haberl, F., "The magnificent seven: magnetic fields and surface temperature distributions," *Ap&SS,* **308**, 181–190 (Apr. 2007).

[13] Borghese, A., Rea, N., Coti Zelati, F., Tiengo, A., Turolla, R., and Zane, S., "Narrow phase-dependent features in X-ray dim isolated neutron stars: a new detection and upper limits," *MNRAS,* **468**, 2975–2983 (July 2017).

[14] Hohle, M. M., Haberl, F., Vink, J., de Vries, C. P., and Neuhäuser, R., "Narrow absorption features in the co-added XMM-Newton RGS spectra of isolated neutron stars," *MNRAS,* **419**, 1525–1536 (Jan. 2012).

[15] Suleimanov, V., Potekhin, A. Y., and Werner, K., "Models of magnetized neutron star atmospheres: thin atmospheres and partially ionized hydrogen atmospheres with vacuum polarization," *A&A,* **500**, 891–899 (Jun 2009).

[16] Potekhin, A. Y., Suleimanov, V. F., van Adelsberg, M., and Werner, K., "Radiative properties of magnetic neutron stars with metallic surfaces and thin atmospheres," *A&A,* **546**, A121 (Oct. 2012).

[17] Heyl, J. S. and Shaviv, N. J., "QED and the high polarization of the thermal radiation from neutron stars," *PhysRevD,* **66**, 023002–+ (July 2002).

[18] Heyl, J. S., Shaviv, N. J., and Lloyd, D., "The high-energy polarization-limiting radius of neutron star magnetospheres - i. slowly rotating neutron stars," *Monthly Notices of the Royal Astronomical Society* **342**(1), 134–144 (2003).

[19] Taverna, R., Turolla, R., Gonzalez Caniulef, D., Zane, S., Muleri, F., and Soffitta, P., "Polarization of neutron star surface emission: a systematic analysis," *MNRAS,* **454**, 3254–3266 (Dec 2015).

[20] Staubert, R., Trümper, J., Kendziorra, E., Klochkov, D., Postnov, K., Kretschmar, P., Pottschmidt, K., Haberl, F., Rothschild, R. E., Santangelo, A., Wilms, J., Kreykenbohm, I., and Fürst, F., "Cyclotron lines in highly magnetized neutron stars," *A&A,* **622**, A61 (Feb 2019).

[21] Meszaros, P., Novick, R., Szentgyorgyi, A., Chanan, G. A., and Weisskopf, M. C., "Astrophysical implications and observational prospects of X-ray polarimetry," *ApJ,* **324**, 1056–1067 (Jan. 1988).

[22] Hickox, R. C. and Vrtilek, S. D., "Pulse-Phase Spectroscopy of SMC X-1 with Chandra and XMM-Newton: Reprocessing by a Precessing Disk?," *ApJ,* **633**, 1064–1075 (Nov. 2005).

[23] Chandrasekhar, S., [*Radiative transfer*], Dover Publications Inc: New York (1960).

[24] Marscher, A. P., "Relativistic jets and the continuum emission in QSOs," *ApJ,* **235**, 386–391 (Jan. 1980).

[25] Giroletti, M., Giovannini, G., Feretti, L., Cotton, W. D., Edwards, P. G., Lara, L., Marscher, A. P., Mattox, J. R., Piner, B. G., and Venturi, T., "Parsec-Scale Properties of Markarian 501," *ApJ,* **600**, 127–140 (Jan. 2004).

[26] Marscher, A. P. and Gear, W. K., "Models for high-frequency radio outbursts in extragalactic sources, with application to the early 1983 millimeter-to-infrared flare of 3C 273," *ApJ,* **298**, 114–127 (Nov. 1985).

[27] Perlman, E. S., Biretta, J. A., Zhou, F., Sparks, W. B., and Macchetto, F. D., "Optical and Radio Polarimetry of the M87 Jet at 0.2" Resolution," *AJ,* **117**, 2185–2198 (May 1999).

[28] Avachat, S. S., Perlman, E. S., Adams, S. C., Cara, M., Owen, F., Sparks, W. B., and Georganopoulos, M., "Multi-wavelength Polarimetry and Spectral Study of the M87 Jet During 2002-2008," *ApJ,* **832**, 3 (Nov 2016).

[29] Marshall, H. L., Miller, B. P., Davis, D. S., Perlman, E. S., Wise, M., Canizares, C. R., and Harris, D. E., "A High-Resolution X-Ray Image of the Jet in M87," *ApJ,* **564**, 683–687 (Jan 2002).

[30] Gallo, L., "X-ray perspective of Narrow-line Seyfert 1 galaxies," in [*Revisiting Narrow-Line Seyfert 1 Galaxies and their Place in the Universe*], 34 (Apr. 2018).

[31] Arnaud, K. A., Branduardi-Raymont, G., Culhane, J. L., Fabian, A. C., Hazard, C., McGlynn, T. A., Shafer, R. A., Tennant, A. F., and Ward, M. J., "EXOSAT observations of a strong soft X-ray excess in MKN 841.," *MNRAS,* **217**, 105–113 (Nov. 1985).

[32] Haardt, F. and Matt, G., "X-ray polarization in the two-phase model for AGN and X-ray binaries," *MNRAS,* **261**, 346–352 (Mar. 1993).

[33] Marin, F., Goosmann, R. W., Dovčiak, M., Muleri, F., Porquet, D., Grosso, N., Karas, V., and Matt, G., "X-ray polarimetry as a new tool to discriminate reflection from absorption scenarios - predictions for MCG-6-30-15," *MNRAS,* **426**, L101–L105 (Oct. 2012).

[34] Walter, R. and Fink, H. H., "The ultraviolet to soft X-ray bump of Seyfert 1 type active galactic nuclei.," *A&A,* **274**, 105 (July 1993).

[35] Boller, T., Brandt, W. N., and Fink, H., "Soft X-ray properties of narrow-line Seyfert 1 galaxies.," *A&A,* **305**, 53–+ (Jan. 1996).

[36] Gierliński, M. and Done, C., "Is the soft excess in active galactic nuclei real?," *MNRAS,* **349**, L7–L11 (Mar. 2004).

[37] Crummy, J., Fabian, A. C., Gallo, L., and Ross, R. R., "An explanation for the soft X-ray excess in active galactic nuclei," *MNRAS,* **365**, 1067–1081 (Feb. 2006).

[38] Komossa, S., "Tidal disruption of stars by supermassive black holes: Status of observations," *Journal of High Energy Astrophysics* **7**, 148–157 (Sept. 2015).

[39] D'Ammando, F., "Short time-scale variability of γ-ray-emitting narrow-line Seyfert 1 galaxies in optical and UV bands," *MNRAS,* **498**, 859–874 (Aug. 2020).

[40] Berton, M., Congiu, E., Järvelä, E., Antonucci, R., Kharb, P., Lister, M. L., Tarchi, A., Caccianiga, A., Chen, S., Foschini, L., Lähteenmäki, A., Richards, J. L., Ciroi, S., Cracco, V., Frezzato, M., La Mura, G., and Rafanelli, P., "Radio-emitting narrow-line Seyfert 1 galaxies in the JVLA perspective," *A&A,* **614**, A87 (June 2018).

[41] Pasham, D. R. and van Velzen, S., "Discovery of a Time Lag between the Soft X-Ray and Radio Emission of the Tidal Disruption Flare ASASSN-14li: Evidence for Linear Disk-Jet Coupling," *ApJ,* **856**, 1 (Mar. 2018).

[42] De Colle, F. and Lu, W., "Jets from Tidal Disruption Events," *New Astronomy Reviews* **89**, 101538 (Sept. 2020).

[43] Wilkins, D. R. and Gallo, L. C., "Driving extreme variability: the evolving corona and evidence for jet launching in Markarian 335," *MNRAS,* **449**, 129–146 (May 2015).

[44] Jin, C., Done, C., and Ward, M., "Re-observing the NLS1 Galaxy RE J1034+396. II. New Insights on the Soft X-ray Excess, QPO and the Analogy with GRS 1915+105," *arXiv e-prints* , arXiv:2007.14704 (July 2020).

[45] Weisskopf, M. C., Elsner, R. F., and O'Dell, S. L., "On understanding the figures of merit for detection and measurement of x-ray polarization," in [*Society of Photo-Optical Instrumentation Engineers (SPIE) Conference Series*], Arnaud, M., Murray, S. S., and Takahashi, T., eds., *Space Telescopes and Instrumentation 2010: Ultraviolet to Gamma Ray* **7732**, 77320E, SPIE (2010).

[46] Chauvin, M., Florén, H.-G., Friis, M., Jackson, M., Kamae, T., Kataoka, J., Kawano, T., Kiss, M., Mikhalev, V., Mizuno, T., Ohashi, N., Stana, T., Tajima, H., Takahashi, H., Uchida, N., and Pearce, M., "Accretion geometry of the black-hole binary Cygnus X-1 from X-ray polarimetry," *Nature Astronomy* **2**, 652–655 (June 2018).

[47] Marshall, H. L., Günther, H. M., Heilmann, R. K., Schulz, N. S., Egan, M., Hellickson, T., Heine, S. N. T., Windt, D. L., Gullikson, E. M., Ramsey, B. D., Tagliaferri, G., and Pareschi, G., "Design of a Broad-band Soft X-ray Polarimeter," *Journal of Astronomical Telescopes, Instruments, and Systems* **4**, 11004 (Mar. 2018).

[48] Zhang, W. W., Allgood, K. D., Biskach, M. P., Chan, K.-W., Hlinka, M., Kearney, J. D., Mazzarella, J. R., McClelland, R. S., Numata, A., Riveros, R. E., Saha, T. T., and Solly, P. M., "High-resolution, lightweight, and low-cost x-ray optics for the Lynx observatory," *Journal of Astronomical Telescopes, Instruments, and Systems* **5**, 021012 (Apr 2019).

[49] Oegelman, H., Finley, J. P., and Zimmerman, H. U., "Pulsed X-rays from the VELA pulsar," *Nature,* **361**, 136–138 (Jan. 1993).

[50] Cash, W., "X-ray optics - A technique for high resolution imaging," *Appl.Optics,* **26**, 2915–2920 (July 1987).

[51] Heilmann, R. K., Ahn, M., Bautz, M. W., Foster, R., Huenemoerder, D. P., Marshall, H. L., Mukherjee, P., Schattenburg, M. L., Schulz, N. S., and Smith, M., "Development of a critical-angle transmission grating spectrometer for the International X-Ray Observatory," in [*Optics for EUV, X-Ray, and Gamma-Ray Astronomy IV*], *SPIE Conference Series,* **7437**, 74370G (Aug. 2009).

[52] Heilmann, R. K., Bruccoleri, A. R., and Schattenburg, M. L., "High-efficiency blazed transmission gratings for high-resolution soft x-ray spectroscopy," in [*Society of Photo-Optical Instrumentation Engineers (SPIE) Conference Series*], *SPIE Conference Series,* **9603**, 960314 (Sept. 2015).

[53] Heilmann, R. K., Bruccoleri, A. R., Song, J., Kolodziejczak, J., Gaskin, J. A., O'Dell, S. L., Cheimetz, P., Hertz, E., Smith, R. K., Burwitz, V., Hartner, G., La Caria, M.-M., and Schattenburg, M. L., "Critical-angle transmission grating technology development for high resolving power soft x-ray spectrometers on Arcus and Lynx," in [*Society of Photo-Optical Instrumentation Engineers (SPIE) Conference Series*], *Society of Photo-Optical Instrumentation Engineers (SPIE) Conference Series* **10399**, 1039914 (Aug. 2017).

[54] Smith, R. K., Abraham, M., Allured, R., Bautz, M., Bookbinder, J., Bregman, J., Brenneman, L., Brickhouse, N. S., Burrows, D., Burwitz, V., Cheimets, P. N., Costantini, E., Dawson, S., DeRoo, C., Falcone, A., Foster, A. R., Gallo, L., Grant, C. E., Günther, H. M., Heilmann, R. K., Hertz, E., Hine, B., Huenemoerder, D., Kaastra, J. S., Kreykenbohm, I., Madsen, K. K., McEntaffer, R., Miller, E., Miller, J., Morse, E., Mushotzky, R., Nandra, K., Nowak, M., Paerels, F., Petre, R., Poppenhaeger, K., Ptak, A., Reid, P., Sanders, J., Schattenburg, M., Schulz, N., Smale, A., Temi, P., Valencic, L., Walker, S., Willingale, R., Wilms, J., and Wolk, S. J., "Arcus: exploring the formation and evolution of clusters, galaxies, and stars," in [*Society of Photo-Optical Instrumentation Engineers (SPIE) Conference Series*], *Society of Photo-Optical Instrumentation Engineers (SPIE) Conference Series* **10397**, 103970Q (Aug. 2017).

[55] Song, J., Heilmann, R. K., Bruccoleri, A. R., Hertz, E., and Schatternburg, M. L., "Scanning laser reflection tool for alignment and period measurement of critical-angle transmission gratings," in [*Society of Photo-Optical Instrumentation Engineers (SPIE) Conference Series*], *Society of Photo-Optical Instrumentation Engineers (SPIE) Conference Series* **10399**, 1039915 (Aug. 2017).

[56] Marshall, H. L., Schulz, N. S., Windt, D. L., Gullikson, E. M., Blake, E., Getty, D., and McInturff, Z., "The use of laterally graded multilayer mirrors for soft X-ray polarimetry," in [*Society of Photo-Optical Instrumentation Engineers (SPIE) Conference Series*], *SPIE Conference Series,* **9144**, 1 (July 2014).

[57] Marshall, H. L., Schulz, N. S., Windt, D. L., Gullikson, E. M., Craft, M., Blake, E., and Ross, C., "The use of laterally graded multilayer mirrors for soft x-ray polarimetry," in [*Society of Photo-Optical Instrumentation Engineers (SPIE) Conference Series*], *SPIE Conference Series,* **9603**, 960319 (Sept. 2015).

[58] LaMarr, B., Grant, C., Kissel, S., Prigozhin, G., Bautz, M., Tsuru, T. G., Tsunemi, H., Dotani, T., Hayashida, K., and Matsumoto, H., "Front- and back-illuminated x-ray CCD performance in low- and high-Earth orbit: performance trends of Suzaku XIS and Chandra ACIS detectors," in [*Space Telescopes and Instrumentation 2008: Ultraviolet to Gamma Ray*], *SPIE Conference Series,* **7011**, 70112C (July 2008).

[59] Günther, H. M., Frost, J., and Theriault-Shay, A., "MARXS: A Modular Software to Ray-trace X-Ray Instrumentation," *AJ,* **154**, 243 (Dec. 2017).

[60] Bautz, M. W., Miller, E. D., Sanders, J. S., Arnaud, K. A., Mushotzky, R. F., Porter, F. S., Hayashida, K., Henry, J. P., Hughes, J. P., Kawaharada, M., Makashima, K., Sato, M., and Tamura, T., "Suzaku Observations of Abell 1795: Cluster Emission to r$_{200}$," *PASJ,* **61**, 1117 (Oct. 2009).

[61] Murphy, K. D., Marshall, H. L., Schulz, N. S., Jenks, K., Sommer, S. J. B., and Marshall, E. A., "Soft x-ray polarimeter laboratory tests," in [*Space Telescopes and Instrumentation 2010: Ultraviolet to Gamma Ray*], *Society of Photo-Optical Instrumentation Engineers (SPIE) Conference Series* **7732**, 77322Y (July 2010).

[62] Marshall, H. L., Schulz, N. S., Remlinger, B., Gentry, E. S., Windt, D. L., and Gullikson, E. M., "Progress toward a soft x-ray polarimeter," in [*Society of Photo-Optical Instrumentation Engineers (SPIE) Conference Series*], *SPIE Conference Series,* **8861** (Sept. 2013).

[63] Garner, A., Marshall, H., Heine, S., Heilmann, R., Song, J., Schulz, N., LaMarr, B., and Egan, M., "Component testing for x-ray spectroscopy and polarimetry," in [*Society of Photo-Optical Instrumentation Engineers (SPIE) Conference Series*], *SPIE Conference Series,* **11118**, 1111811–1–12 (Sept. 2019).

[64] Schwartz, D. A., Vikhlinin, A., Tananbaum, H., Freeman, M., Tremblay, G., Schwartz, E. D., Gaskin, J. A., Swartz, D., Gelmis, K., McCarley, K. S., and Dominguez, A., "The Lynx X-ray Observatory: revealing the invisible universe," in [*UV, X-Ray, and Gamma-Ray Space Instrumentation for Astronomy XXI*], *Society of Photo-Optical Instrumentation Engineers (SPIE) Conference Series* **11118**, 111180K (Sept. 2019).

[65] Bautz, M. W., "The Lynx X-Ray Observatory: Science Drivers," in [*UV, X-Ray, and Gamma-Ray Space Instrumentation for Astronomy XXI*], *Society of Photo-Optical Instrumentation Engineers (SPIE) Conference Series* **11118**, 111180J (Sept. 2019).

[66] Jahoda, K., Krawczynski, H., Kislat, F., Marshall, H., Okajima, T., Agudo, I., Angelini, L., Bachetti, M., Baldini, L., Baring, M., Baumgartner, W., Bellazzini, R., Bianchi, S., Bucciantini, N., Caiazzo, I., Capitanio, F., Coppi, P., Costa, E., De Rosa, A., Del Monte, E., Dexter, J., Di Gesu, L., Di Lalla, N., Doroshenko, V., Dovciak, M., Ferrazzoli, R., Fuerst, F., Garner, A., Ghosh, P., Gonzalez-Caniulef, D., Grinberg, V., Gunji, S., Hartman, D., Hayashida, K., Heyl, J., Hill, J., Ingram, A., Buz Iwakiri, W., Jorstad, S., Kaaret, P., Kallman, T., Karas, V., Khabibullin, I., Kitaguchi, T., Kolodziejczak, J., Kouveliotou, C., Liodakis, Y., Maccarone, T., Manfreda, A., Marin, F., Marinucci, A., Markwardt, C., Marscher, A., Matt, G., McConnell, M., Miller, J., Mitsubishi, I., Mizuno, T., Mushtukov, A., Ng, S., Nowak, M., O'Dell, S., Papitto, A., Pasham, D., Pearce, M., Peirson, L., Perri, M., Pesce Rollins, M., Petrosian, V., Petrucci, P.-O., Pilia, M., Possenti, A., Poutanen, J., Prescod-Weinstein, C., Puccetti, S., Salmi, T., Shi, K., Soffita, P., Spandre, G., Steiner, J., Strohmayer, T., Suleimanov, V., Svoboda, J., Swank, J., Tamagawa, T., Takahashi, H., Taverna, R., Tomsick, J., Trois, A., Tsygankov, S., Turolla, R., Vink, J., Wilms, J., Wu, K., Xie, F., Younes, G., Zaino, A., Zajczyk, A., Zane, S., Zdziarski, A., Zhang, H., Zhang, W., and Zhou, P., "The X-ray Polarization Probe mission concept," *arXiv e-prints* , arXiv:1907.10190 (Jul 2019).

[67] Kislat, F., Abarr, Q., Beheshtipour, B., Geronimo, G. D., Dowkontt, P., Tang, J., and Krawczynski, H., "Optimization of the design of X-Calibur for a long-duration balloon flight and results from a one-day test flight," *Journal of Astronomical Telescopes, Instruments, and Systems* **4**(1), 1 – 9 (2018).

[68] Krawczynski, H., Matt, G., Ingram, A. R., Taverna, R., Turolla, R., Kislat, F., Teddy Cheung, C. C., Bykov, A., Sinha, K., Zhang, H., Heyl, J., Bucciantini, N., Madejski, G., Kallman, T., Jahoda, K. M., Abarr, Q., Baring, M. G., Baldini, L., Begelman, M., Boettcher, M., Cackett, E., Caiazzo, I., Coppi, P., Costa, E., Dexter, J., Fortin, J.-F., Gammie, C., Gaskin, J. A., Giannios, D., Ghosh, P., Harding, A. K., Hartmann, D. H., Hayashida, K., Jorstad, S. G., Kaaret, P., Kitaguchi, T., Latronico, L., Maccarone, T., Marscher, A., Marshall, H., McConnell, M., Miller, J. M., O'Dell, S. L., Oezel, F., Okajima, T., Pearce, M., Perkins, J., Ramsey, B. D., Romani, R. W., Schnittman, J. D., Sgro, C., Soffitta, P., Takahashi, H., Tamagawa, T.,

Tomsick, J., Weisskopf, M. C., and Younes, G., "Astro2020 Science White Paper: Using X-Ray Polarimetry to Probe the Physics of Black Holes and Neutron Stars," *arXiv e-prints* , arXiv:1904.09313 (Apr 2019).